

This is an Open Access document downloaded from ORCA, Cardiff University's institutional repository: <https://orca.cardiff.ac.uk/id/eprint/121286/>

This is the author's version of a work that was submitted to / accepted for publication.

Citation for final published version:

Narangari, Parvathala Reddy, Karuturi, Siva Krishna, Wu, Yiliang, Wong-Leung, Jennifer, Vora, Kaushal, Lysevych, Mykhaylo, Wan, Yimao, Tan, Hark Hoe, Jagadish, Chennupati and Mokkalapati, Sudha 2019. Ultrathin Ta<sub>2</sub>O<sub>5</sub> electron-selective contacts for high efficiency InP solar cells. *Nanoscale* 11 (15) , pp. 7497-7505. 10.1039/C8NR09932D

Publishers page: <http://dx.doi.org/10.1039/C8NR09932D>

Please note:

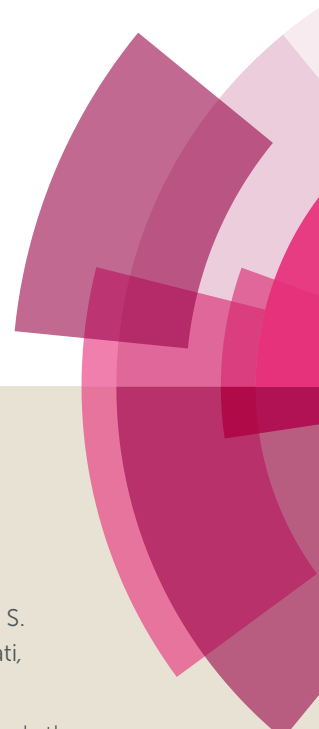
Changes made as a result of publishing processes such as copy-editing, formatting and page numbers may not be reflected in this version. For the definitive version of this publication, please refer to the published source. You are advised to consult the publisher's version if you wish to cite this paper.

This version is being made available in accordance with publisher policies. See <http://orca.cf.ac.uk/policies.html> for usage policies. Copyright and moral rights for publications made available in ORCA are retained by the copyright holders.

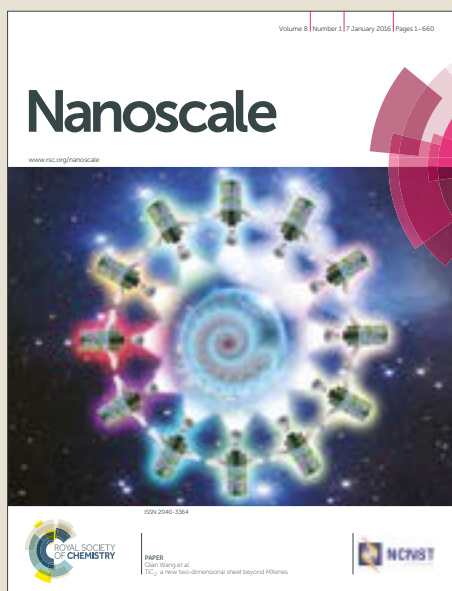


# Nanoscale

Accepted Manuscript



This article can be cited before page numbers have been issued, to do this please use: P. R. Narangari, S. K. Karuturi, Y. Wu, J. Wong-Leung, K. Vora, M. Lysevych, Y. Wan, H. H. Tan, C. Jagadish and S. Mokkalapati, *Nanoscale*, 2019, DOI: 10.1039/C8NR09932D.



This is an Accepted Manuscript, which has been through the Royal Society of Chemistry peer review process and has been accepted for publication.

Accepted Manuscripts are published online shortly after acceptance, before technical editing, formatting and proof reading. Using this free service, authors can make their results available to the community, in citable form, before we publish the edited article. We will replace this Accepted Manuscript with the edited and formatted Advance Article as soon as it is available.

You can find more information about Accepted Manuscripts in the [author guidelines](#).

Please note that technical editing may introduce minor changes to the text and/or graphics, which may alter content. The journal's standard [Terms & Conditions](#) and the ethical guidelines, outlined in our [author and reviewer resource centre](#), still apply. In no event shall the Royal Society of Chemistry be held responsible for any errors or omissions in this Accepted Manuscript or any consequences arising from the use of any information it contains.

# Ultrathin Ta<sub>2</sub>O<sub>5</sub> Electron-Selective Contacts for High Efficiency InP Solar Cells

View Article Online  
DOI: 10.1039/C9NR09932D

Parvathala Reddy Narangari<sup>1</sup>, Siva Krishna Karuturi<sup>1, 2\*</sup>, Yiliang Wu<sup>2</sup>, Jennifer Wong Leung<sup>1</sup>, Kaushal Vora<sup>3</sup>, Mykhaylo Lysevych<sup>1</sup>, Yimao Wan<sup>2</sup>, H. H. Tan<sup>1</sup>, C. Jagadish<sup>1</sup> and S. Mokkalapati<sup>3\*</sup>

<sup>1</sup> Department of Electronic Materials Engineering, Research School of Physics and Engineering, Australian National University, Canberra, ACT 2601, Australia.

<sup>2</sup> Research School of Engineering, Australian National University, Canberra, ACT 2601, Australia.

<sup>3</sup> School of Physics and Astronomy, Cardiff University, Parade, Cardiff, United Kingdom, CF24 3AA.

\* Corresponding authors: [siva.karuturi@anu.edu.au](mailto:siva.karuturi@anu.edu.au) and [MokkalapatiS@Cardiff.ac.uk](mailto:MokkalapatiS@Cardiff.ac.uk)

## ABSTRACT

Heterojunction solar cells with transition-metal-oxide-based carrier-selective contacts have been gaining considerable research interest owing to their amenability to low-cost fabrication methods and elimination of parasitic absorption and complex semiconductor doping process. In this work, we propose tantalum oxide (Ta<sub>2</sub>O<sub>5</sub>) as a novel electron-selective contact layer for photo-generated carrier separation in InP solar cells. We confirm the electron-selective properties of Ta<sub>2</sub>O<sub>5</sub> by investigating band energetics at the InP-Ta<sub>2</sub>O<sub>5</sub> interface using X-ray photoelectron spectroscopy. Time-resolved photoluminescence and power dependent photoluminescence reveal that the Ta<sub>2</sub>O<sub>5</sub> inter-layer also mitigates parasitic recombination at the InP/transparent conducting oxide interface. With an 8 nm Ta<sub>2</sub>O<sub>5</sub> layer deposited using an atomic layer deposition (ALD) system, we demonstrate a planar InP solar cell with an open circuit voltage, V<sub>oc</sub>, of 822 mV, a short circuit current density, J<sub>sc</sub>, of 30.1 mA/cm<sup>2</sup>, and a fill factor of 0.77, resulting in an overall device efficiency of 19.1%. The V<sub>oc</sub> is the highest reported value to date for an InP heterojunction solar cells with carrier-selective contacts. The proposed Ta<sub>2</sub>O<sub>5</sub> material may be of interest not only for other solar cell architectures including perovskite cells and organic solar cells, but also across a wide range of optoelectronics applications including solid state emitting devices, photonic crystals, planar light wave circuits etc.

## INTRODUCTION

The direct conversion of sunlight into electricity makes solar cells one of the most promising renewable energy technologies as solar energy is an abundant, inexhaustible clean-energy resource. III-V semiconductors are considered ideal candidates for high efficiency solar cells owing to their direct band gaps, high optical absorption, longer minority carrier lifetimes and high mobilities. Among III-V compounds, InP and GaAs possess optimal band gaps for high efficiency solar cells<sup>1-2</sup>. So far, the best reported efficiencies for single homojunction GaAs and InP solar cells are  $28.8 \pm 0.9\%$ <sup>2-3</sup> and  $22.1 \pm 0.7\%$ <sup>2, 4-5</sup> respectively, making GaAs the highest efficiency single junction solar cell to date. Despite achieving high efficiencies, III-V solar cells are still limited to non-terrestrial applications due to the scarcity of materials and very high costs involved in device processing. At present, considerable research is devoted to the reduction of device costs while maintaining high efficiencies. This can be achieved through the development of cost-effective materials and the use of low-cost processing such as non-epitaxial thin films<sup>6</sup> and epitaxial lift-off processes<sup>7-9</sup>. Heterojunction device architectures with carrier-selective contacts hold the key to realising high efficiency photovoltaics via simple and cost-effective approaches<sup>10-11</sup>.

The two basic mechanisms that constitute the operation of a solar cell are: (i) electron-hole pair generation in a semiconductor by the absorption of photons and (ii) separation and extraction of photo-generated carriers to generate a current in the external circuit. In order to achieve the limiting solar cell efficiency for a given absorber, predicted by Shockley and Queisser<sup>12</sup> using thermodynamic considerations, the absorption in the semiconductor, and therefore electron-hole pair generation needs to be maximized and the photo-generated carriers need to be extracted at the quasi-Fermi levels. In inorganic solar cells (Si and III-Vs), the photo-generated electrons and holes are conventionally swept away to different regions of the solar cell by creating electric field gradients inside the semiconductor by selectively introducing p- and n-type dopants to form a p-n junction<sup>13</sup>. P-n junctions, however, do not extract photo-generated carriers at the quasi-Fermi levels, resulting in lower than predicted open-circuit voltages in solar cells. Further, the heavy doping of semiconductors to increase conductivity causes an increase in non-radiative recombination, a decrease in carrier mobility, a decrease in contact selectivity, and an increase in minority carrier conductivity due to parasitic absorption, all of which are detrimental to the solar cell performance<sup>14-18</sup>. Developing electron and hole-selective

contacts or electron-transparent, hole-blocking and electron-blocking, hole-transparent layers may enable photo-generated carrier extraction from solar cells at the quasi-Fermi levels<sup>19-20</sup>.

The electron (hole) selective layer should have a band alignment with the absorber semiconductor such that there is no impediment to electron (hole) transfer into the selective layer, but a large valence (conduction) band offset that reflects holes (electrons)<sup>13, 21-22</sup>.

Development of electron-selective and hole-selective contacts will enable the realisation of p-n junction-less solar cells. This concept is relatively new in the context of inorganic (Si and III-V) solar cells. However, organic solar cells, perovskite solar cells and dye sensitized solar cells have always used this approach for photo-generated carrier extraction at the contacts. Carrier-selective contacts offer simultaneous passivation with a high degree of carrier selectivity and eliminate parasitic absorption within the heterocontacts. Recently, there are an increasing number of reports investigating carrier-selective contacts for inorganic solar cells<sup>21-33</sup>. NiO, WO<sub>x</sub>, MoO<sub>x</sub>, and CrO<sub>x</sub> have been studied as hole-selective, electron-blocking layers for Si<sup>23, 26-27, 34-39</sup> and GaAs<sup>35</sup> absorbers. TiO<sub>2</sub>, TaO<sub>x</sub> and TaN<sub>x</sub> have been investigated as electron-selective, hole-blocking layers for Si<sup>30-33, 38, 40</sup> and InP<sup>10, 28</sup> absorbers. Battaglia *et al.*<sup>22</sup> observed reduced parasitic absorption for Si solar cells featuring MoO<sub>x</sub> as a hole-selective contact, which resulted in an increased photocurrent density. Wan *et al.*<sup>30-31</sup> reported power conversion efficiencies exceeding 20% for crystalline silicon solar cells by employing magnesium oxide (MgO<sub>x</sub>) and magnesium fluoride (MgF<sub>x</sub>) as electron-selective contacts. Most recently, Yang *et al.*<sup>32</sup> demonstrated over 20% power conversion efficiency for n-type c-Si solar cells using tantalum nitride (TaN<sub>x</sub>) as an electron-selective contact. The significant improvement in the open-circuit voltage and fill factor due to improved passivation and reduced contact resistivity contributed to the improved power-conversion efficiency of the solar cells. Despite several reports on silicon solar cells with carrier-selective contacts, to the best of our knowledge very limited work has been reported on InP heterojunction solar cells with carrier-selective contacts. So far, Yin *et al.*<sup>10</sup> has demonstrated the highest ever reported power conversion efficiency of 19.2% for InP heterojunction solar cells with TiO<sub>2</sub> as an electron-selective contact. They further investigated the influence of the material quality of TiO<sub>2</sub> on solar cell performance and found that 10 nm of TiO<sub>2</sub> in the amorphous phase is optimal to achieve a maximum open-circuit voltage of 780 mV.

In this manuscript, we propose and demonstrate Ta<sub>2</sub>O<sub>5</sub> as an efficient electron-selective, hole blocking layer for InP solar cells. Ta<sub>2</sub>O<sub>5</sub> is an extremely potent and stable material that has been used in anti-reflection coatings, multi-layer interference filters and DRAM capacitors<sup>41-</sup>

<sup>43</sup>, owing to its large refractive index and dielectric constant. Ta<sub>2</sub>O<sub>5</sub> is also transparent to incident solar radiation due to its large band gap<sup>44-46</sup>. It has been shown that Ta<sub>2</sub>O<sub>5</sub> has good electron conductivity due to defects that can be controlled via doping<sup>46</sup>. These properties make Ta<sub>2</sub>O<sub>5</sub> a potential candidate material for electron-selective contacts for inorganic solar cells. Very recently, TaO<sub>x</sub> has been reported as a passivating electron-selective contact for Si solar cells<sup>47</sup>. However, TaO<sub>x</sub> films were subjected to a hydrogenation process before being employed as electron-selective passivation contacts which resulted in a sub-stoichiometric TaO<sub>x</sub> films. Herein, we report for the first time stoichiometric Ta<sub>2</sub>O<sub>5</sub>, using an atomic layer deposition (ALD) system, as an electron-selective contact by demonstrating an InP heterojunction solar cell with a power conversion efficiency of 19.1%, representing 9.4% absolute enhancement over the reference cell without a Ta<sub>2</sub>O<sub>5</sub> layer.

## RESULTS AND DISCUSSION

To investigate the stoichiometry and understand the behavior of Ta<sub>2</sub>O<sub>5</sub> as an electron-selective layer for photo-generated carriers in InP, we performed XPS and UPS measurements on ALD-deposited Ta<sub>2</sub>O<sub>5</sub> on InP. Calibration of XPS and UPS was carried out using a silver (Ag) reference before performing the measurements. Figure 1(a) illustrates the Ta 4f core level XPS spectrum of Ta<sub>2</sub>O<sub>5</sub> measured using 1486.68 eV monochromatic Al K $\alpha$  photons. As shown in Figure 1(a), the 4f core level spectrum is split into a spin-orbit doublet of Ta 4f<sub>7/2</sub> and Ta 4f<sub>5/2</sub>, corresponding to the Ta<sup>5+</sup> valence state. These Ta 4f<sub>7/2</sub> and Ta 4f<sub>5/2</sub> peaks originate at a binding energy of 26.7 and 28.6 eV respectively, with a separation of 1.9 eV. We were able to fit the experimental spectrum using two Gaussian components. No noticeable peaks relating to the Ta<sup>+</sup>, Ta<sup>2+</sup>, Ta<sup>3+/4+</sup> valence states are observed in the Ta 4f core level spectrum towards lower binding energies (< 26.7 eV). These Ta 4f core level spectrum results are in reasonable agreement with the literature<sup>48-49</sup> for Ta<sub>2</sub>O<sub>5</sub> stoichiometry, indicating that our TaO<sub>x</sub> films have the same stoichiometry. Figure 1(b) shows the XPS core level spectrum of O 1s, which is fitted with two Gaussian components centered at 530.9 and 531.8 eV. The small peak located at 531.8 eV is usually attributed to surface contamination<sup>50</sup>. The peak located at the lower binding energy of 530.9 eV is ascribed to Ta-O binding in TaO<sub>x</sub> films<sup>49</sup>. The ratio of areas under the O 1s and Ta 4f core level spectra results in an O to Ta atomic fraction of ~2.51. This further confirms that our ALD-deposited TaO<sub>x</sub> has Ta<sub>2</sub>O<sub>5</sub> stoichiometry.

Figure 1(c) and 1(d) show the XPS valence band spectra of Ta<sub>2</sub>O<sub>5</sub> and InP respectively. The position of the valence band maximum is extracted by linear extrapolation of the valence

band spectrum, while the Fermi level ( $E_F$ ) is located at 0 eV binding energy. As shown in Figure 1(c) and 1(d), linear extrapolation fixes the valence band maxima (VBM) of  $Ta_2O_5$  and InP at 3.36 and 0.69 eV below  $E_F$  respectively. The work function of these materials was determined from UPS spectra using the expression

$$\text{Work function } (\Phi) = h\nu - (E_{\text{cut-off}} - E_F). \quad \dots\dots\dots (1)$$

where  $h\nu$  is the energy of the He-I source (21.2 eV),  $E_{\text{cut-off}}$  is the cut-off of the tail at the higher binding energy end of the UPS spectrum and  $E_F$  is the Fermi energy, which is located at 0 eV. Figure 1(e) shows the UPS spectra of both  $Ta_2O_5$  and InP, from which the work functions of  $Ta_2O_5$  and InP are determined to be same (~5.1 eV), which means that  $E_F$  is placed at 5.1 eV below the vacuum level for both materials. The conduction band minimum (CBM) of  $Ta_2O_5$  deduced from the work function, band gap and position of the VBM below the Fermi level falls at 4.56 eV below the vacuum level. We have used the literature-reported band gap of 3.9 eV<sup>44-45</sup> in determining the CBM of  $Ta_2O_5$ . The information on the Fermi level position below the vacuum level and the VBM below the Fermi level fixes the VBM of  $Ta_2O_5$  at 8.46 eV below the vacuum level. A similar analysis for InP yields the VBM located at 5.79 eV and CBM at 4.44 eV below the vacuum level.

Figure 1(f) shows a schematic of the band alignment at the InP- $Ta_2O_5$  interface calculated using the XPS and UPS data shown in Figure 1(c-e). The Fermi levels in InP and  $Ta_2O_5$  are aligned at equilibrium, resulting in a conduction band offset  $\Delta E_{CB} = [(E_{CB})_{\text{InP}} - (E_{CB})_{\text{Ta}_2\text{O}_5}]$  of 0.12 eV and a valence band offset  $\Delta E_{VB} = [(E_{VB})_{\text{InP}} - (E_{VB})_{\text{Ta}_2\text{O}_5}]$  of 2.67 eV. The conduction band offset favours the transfer of photo-generated electrons in the InP absorber to the  $Ta_2O_5$  layer. The  $\Delta E_{CB}$  is sufficiently larger than the thermal energy of electrons at room temperature to prevent electron transfer back into the InP layer. The large valence band offset of 2.67 eV at the interface prevents or blocks the photo-generated holes from transferring to the  $Ta_2O_5$  layer. Hence the InP- $Ta_2O_5$  interface should act as an efficient electron-selective, hole-blocking layer for photo-generated carriers in InP.

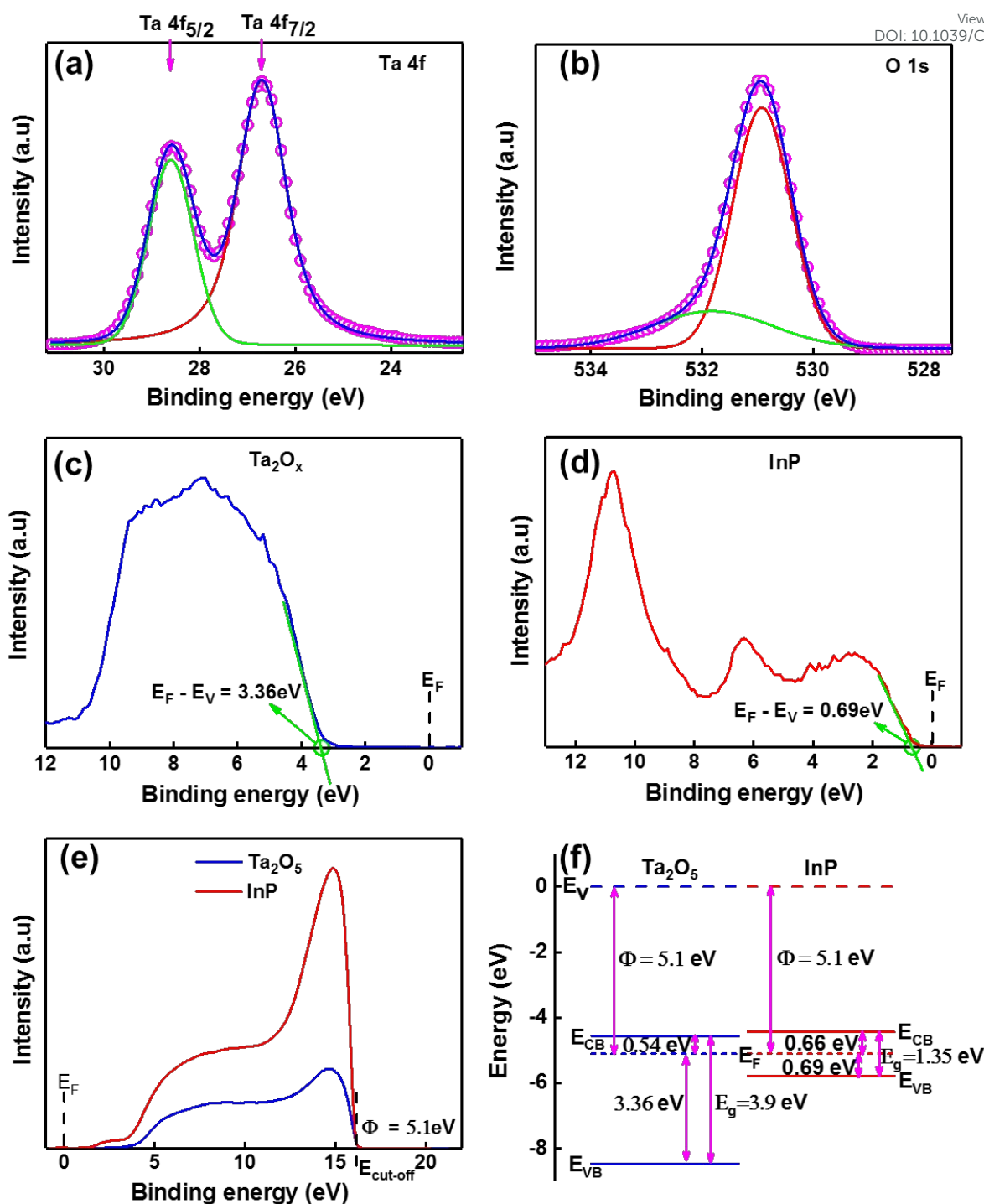


Figure 1. X-ray photoelectron spectra of (a) the Ta 4f core level and (b) the O 1s core level of ALD-deposited Ta<sub>2</sub>O<sub>5</sub> film. XPS valence band spectra of (c) Ta<sub>2</sub>O<sub>5</sub> and (d) InP with the Fermi level ( $E_F$ ) at zero binding energy. (e) UV photoelectron spectrum of Ta<sub>2</sub>O<sub>5</sub> and InP with the Fermi level ( $E_F$ ) at 0 eV. (f) Schematic of the band alignment at the InP-Ta<sub>2</sub>O<sub>5</sub> interface, calculated from data shown in c-e.

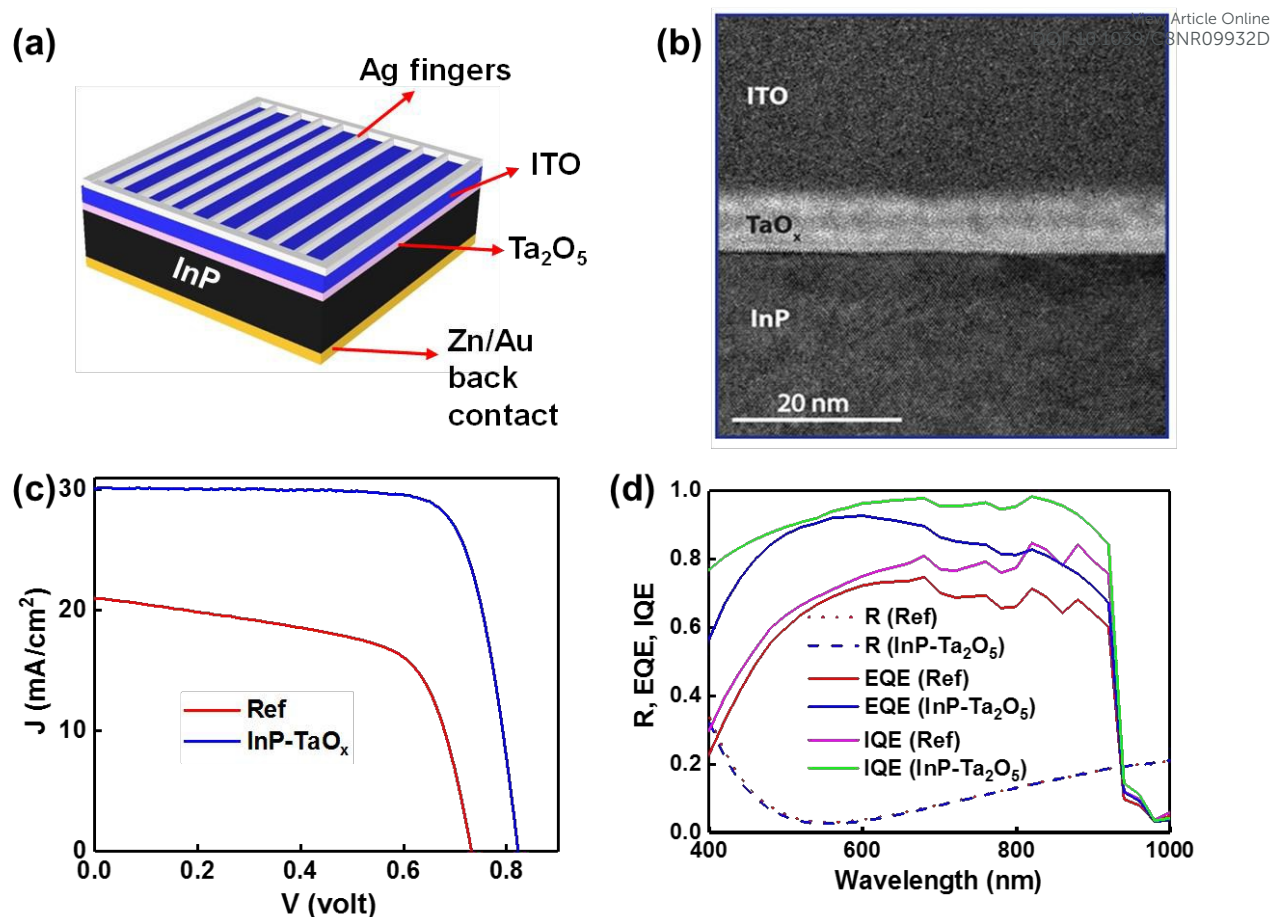


Figure 2. (a) Schematic of the InP solar cell with a Ta<sub>2</sub>O<sub>5</sub> electron-selective layer. (b) High resolution cross-section TEM image of ITO-Ta<sub>2</sub>O<sub>5</sub>-InP interfaces, (c) J-V characteristics of a solar cells under 1 Sun illumination, and (d) Reflectance, EQE and IQE spectra for the reference (InP, without any carrier-selective layer) and the InP-Ta<sub>2</sub>O<sub>5</sub> solar cell.

Figure 2(a) shows a schematic of the simple device structure of the InP solar cell with a Ta<sub>2</sub>O<sub>5</sub> carrier-selective layer, while Figure 2(b) shows a cross-sectional high resolution transmission electron microscope (HRTEM) image of the ITO-Ta<sub>2</sub>O<sub>5</sub>-InP interfaces. TEM analysis shows that the ALD-deposited Ta<sub>2</sub>O<sub>5</sub> layer is amorphous in nature and forms a sharp interface with InP, with an average thickness of ~8 nm. EDS maps of the cross-section of the ITO-Ta<sub>2</sub>O<sub>5</sub>-InP interface confirm the presence of uniform Ta<sub>2</sub>O<sub>5</sub> in the device (as shown in the supporting information (SI) (Figure s2)).

Figure 2(c) shows the J-V (current density vs voltage) characteristics for a reference InP solar cell (InP-ITO) and an InP solar cell with Ta<sub>2</sub>O<sub>5</sub> carrier-selective layer. With the Ta<sub>2</sub>O<sub>5</sub> electron-transparent, hole-blocking layer, the solar cell exhibits higher  $V_{oc}$ ,  $J_{sc}$ , fill factor and efficiency compared to the reference solar cell. The  $V_{oc}$  is increased by 12.4%, from 731 to 822 mV and the  $J_{sc}$  is increased by 43%, from 21.02 to 30.1 mA/cm<sup>2</sup>. The  $V_{oc}$  for the InP-Ta<sub>2</sub>O<sub>5</sub> solar cell is the highest reported value for a heterojunction InP solar cell and is only 6% lower than the

highest reported value for a homojunction (p-n junction) InP solar cell<sup>5</sup>. The fill factor for the InP-Ta<sub>2</sub>O<sub>5</sub> solar cell is 0.77, resulting in an overall device efficiency of 19.1%. The device area for the solar cells reported in this work (1 cm<sup>2</sup>) is 4 times larger than the device area for the InP-TiO<sub>2</sub> heterojunction solar cells (0.25 cm<sup>2</sup>) recently reported by Yin et.al<sup>10</sup>. Despite this, the InP-Ta<sub>2</sub>O<sub>5</sub> solar cell efficiency is comparable to the efficiency of the InP-TiO<sub>2</sub> heterojunction solar cell (19.2%). Table 1 lists and compares the V<sub>oc</sub>, J<sub>sc</sub>, fill factor and efficiency of the InP-Ta<sub>2</sub>O<sub>5</sub> carrier-selective solar cell with a reference solar cell, InP-TiO<sub>2</sub><sup>10</sup>, InP-CdS<sup>11, 51</sup> heterojunction and InP p-n homojunction<sup>5</sup> solar cells.

*Table 1. Performance characteristics for reference InP solar cell (with no carrier-selective layer) and an InP solar cell with a Ta<sub>2</sub>O<sub>5</sub> electron-transparent, hole-blocking layer. Data reported in literature for InP-TiO<sub>2</sub> and InP-CdS heterojunction solar cells and an InP p-n junction solar cell are also shown for comparison.*

Device type	V <sub>oc</sub> (mV)	J <sub>sc</sub> (mA/cm <sup>2</sup> )	Fill factor	Efficiency (%)
Reference	731	21.02	0.63	9.66
InP-Ta <sub>2</sub> O <sub>5</sub>	822	30.1	0.77	19.1
InP-TiO <sub>2</sub> <sup>10</sup>	785	30.5	0.80	19.2
InP-CdS <sup>11, 51</sup>	750	32.3	0.72	17.4
InP p-n junction <sup>5</sup>	878	29.5	0.85	22.1

Figure 2(d) shows the reflectance (R) spectra, the external quantum efficiency (EQE) and the internal quantum efficiency (IQE) data for the reference solar cell and the solar cell with a Ta<sub>2</sub>O<sub>5</sub> carrier-selective layer for the wavelength range 320 – 1000 nm. The IQE data is calculated from the experimentally measured EQE and reflectance spectra using the relation  $IQE = \frac{EQE}{1-R}$ . The maximum short circuit current density for an ideal solar cell assuming 100% absorption of above band gap energy solar radiation in this wavelength range ( $J_{sc-ideal}$ ) calculated using  $J_{sc-ideal} = \int_{320}^{924} \frac{q\lambda}{hc} AM1.5G(\lambda)d\lambda$  is 34.54 mA/cm<sup>2</sup>. The reflectance spectra are for the final devices with ITO and Ag fingers for the top contact. The reflectance spectra for both devices are very similar, suggesting that the differences in device characteristics shown in Figure 2(c) are a consequence of the electronic properties of the device. The maximum  $J_{sc}$  calculated from the reflectance spectra for both solar cells is ~32.8 mA/cm<sup>2</sup>. A short circuit current density of ~1.74 mA/cm<sup>2</sup> or 5% of the ideal  $J_{sc-ideal}$  is lost due to reflection losses from the front contact. The  $J_{sc}$  calculated from the experimentally-determined EQE spectra

shown in Figure 2(d) match closely with the  $J_{sc}$  values measured from J-V characteristics, with less than 3% error for the reference and the InP-Ta<sub>2</sub>O<sub>5</sub> solar cells.

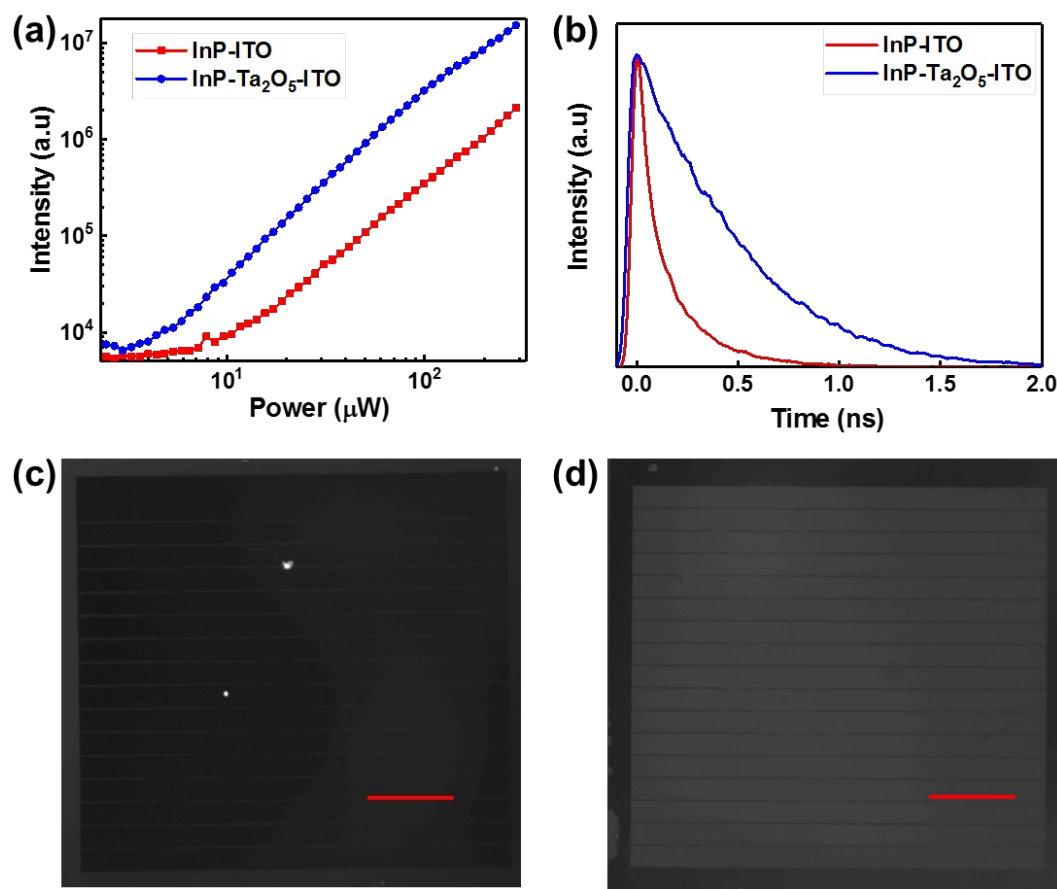


Figure 3. (a) Photoluminescence (PL) intensity versus excitation power and (b) time-resolved PL spectra for InP-ITO and InP-Ta<sub>2</sub>O<sub>5</sub>-ITO samples. PL images of (c) the reference and (d) the InP-Ta<sub>2</sub>O<sub>5</sub>-ITO solar cells (the scale bar is 2 mm).

Photoluminescence (PL) studies were carried out to understand the solar cell performance. Figure 3 compares the PL emission characteristics of InP-ITO and InP-Ta<sub>2</sub>O<sub>5</sub>-ITO samples. The InP-Ta<sub>2</sub>O<sub>5</sub>-ITO sample consistently shows higher PL intensity compared to the InP-ITO sample at all excitation powers (Figure 3(a)). The time-resolved PL curves for the two samples are shown in Figure 3(b). The minority carrier lifetimes extracted for the InP-ITO and InP-Ta<sub>2</sub>O<sub>5</sub>-ITO samples from the time resolved PL data are 138 ps and 494 ps, respectively. The larger emission intensity and longer minority carrier lifetime for the InP-Ta<sub>2</sub>O<sub>5</sub>-ITO sample indicates reduced non-radiative recombination processes at the InP/ITO interface due to the presence of the Ta<sub>2</sub>O<sub>5</sub> layer. The reduced parasitic recombination at the InP surface leads to a  $\sim 9$  mA/cm<sup>2</sup> gain in the  $J_{sc}$  of the solar cell (Figure 2(c)). PL images of the InP-ITO (reference sample) and the InP-Ta<sub>2</sub>O<sub>5</sub>-ITO sample are shown in Figure 3 (c) and 3(d) respectively. The PL images are taken for the solar cells fabricated from the InP-ITO and InP-Ta<sub>2</sub>O<sub>5</sub>-ITO

samples. The front contact fingers can be seen in the images. As expected from the reduced recombination at the InP-ITO interface due to the presence of the Ta<sub>2</sub>O<sub>5</sub> interlayer (and hence longer minority carrier lifetime in the InP-Ta<sub>2</sub>O<sub>5</sub>-ITO sample), the InP-Ta<sub>2</sub>O<sub>5</sub>-ITO sample is brighter compared to the reference sample. Reduced parasitic recombination in the InP-Ta<sub>2</sub>O<sub>5</sub>-ITO sample compared to the reference sample should lead to a higher V<sub>oc</sub>, as is observed experimentally (Figure 2(c)).

The PL results are further used to explain the low IQE of the reference solar cell in the short wavelength region (IQE < 0.6 for  $\lambda < 500$  nm) as shown in Figure 2(d). The IQE increases from 0.28 at 400 nm to 0.77 at 860 nm. From Figure s3 in the SI, the PL intensity and minority carrier lifetime of InP is observed to drop drastically after ITO deposition compared to bare InP. This indicates that ITO deposition caused surface damage to the InP surface. As a result, our reference solar cell exhibits a poor IQE response in the short wavelength region. This is because short wavelength incident light has a very shallow absorption depth (~20 nm for incident wavelength of 400 nm) and extensive surface damage leads to inefficient collection of carriers generated by the absorption of short wavelength light. However, the PL intensity of InP after ITO deposition recovers significantly when Ta<sub>2</sub>O<sub>5</sub> is introduced in between InP and ITO, as shown in Figure s3 in SI. This indicates that Ta<sub>2</sub>O<sub>5</sub> acts as a protection layer in addition to being a carrier separation layer. As a consequence, the InP-Ta<sub>2</sub>O<sub>5</sub> solar cell exhibits larger gains in the IQE at short wavelengths than in the long wavelength region compared to the reference solar cell. The IQE increases from 0.28 to 0.76 at 400 nm, 0.74 to 0.95 at 600 nm and 0.77 to 0.94 at 860 nm. This corresponds to an increase of 171% at 400 nm, 28% at 600 nm and 22% at 860 nm. A large increase in the short wavelength response of the solar cell is due to the reduction of surface damage and efficient carrier separation closer to the InP surface where most short wavelength light is absorbed, due to the presence of the Ta<sub>2</sub>O<sub>5</sub> carrier-selective layer.

Figure 4 shows the variation of the InP-Ta<sub>2</sub>O<sub>5</sub> solar cell performance characteristics (J<sub>sc</sub>, V<sub>oc</sub>, FF and efficiency) with the thickness of the Ta<sub>2</sub>O<sub>5</sub> layer. The characteristic parameters for the reference solar cell are also shown (i.e. at a thickness of 0 nm). The J<sub>sc</sub>, V<sub>oc</sub>, FF and efficiency of the solar cell first increase with the thickness of the Ta<sub>2</sub>O<sub>5</sub> layer and then decrease beyond a thickness of 8 nm. The reverse saturation current densities, J<sub>0</sub> extracted from the dark J-V data (please see Figure s4 in SI) for the InP-ITO solar cell, InP-5 nm Ta<sub>2</sub>O<sub>5</sub> solar cell and InP-8 nm Ta<sub>2</sub>O<sub>5</sub> are 37  $\mu\text{A}/\text{cm}^2$ , 60  $\text{nA}/\text{cm}^2$  and 0.1  $\text{nA}/\text{cm}^2$ , respectively. The reverse saturation current density decreases with increasing thickness of the Ta<sub>2</sub>O<sub>5</sub> layer, indicating that a thicker Ta<sub>2</sub>O<sub>5</sub>

layer acts as a better barrier against InP surface damage due to ITO deposition. However, thick Ta<sub>2</sub>O<sub>5</sub> layers also exhibit increased resistance to electron flow to the metal contact. The series resistance  $R_s$  of the solar cell increases from 3  $\Omega$  cm<sup>2</sup> for 8 nm of Ta<sub>2</sub>O<sub>5</sub> to 67  $\Omega$  cm<sup>2</sup> for 12 nm of Ta<sub>2</sub>O<sub>5</sub>. Hence there exists an optimal thickness of  $\sim$ 8 nm for the Ta<sub>2</sub>O<sub>5</sub> layer to maximize the efficiency of the solar cell. However, doping the Ta<sub>2</sub>O<sub>5</sub> layer to increase its electron conductivity<sup>46</sup> may alleviate the issue of increasing  $R_s$  and result in better performance for thicker Ta<sub>2</sub>O<sub>5</sub> layers.

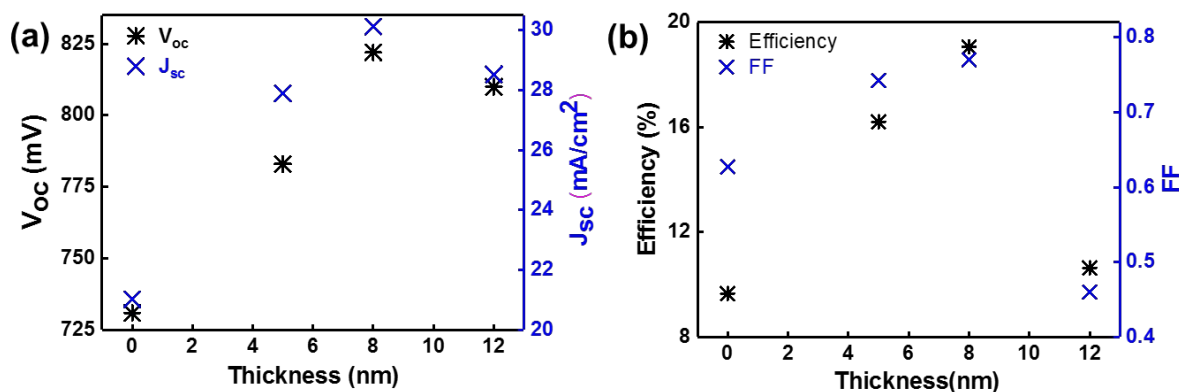


Figure 4. Variation of InP-Ta<sub>2</sub>O<sub>5</sub> solar cell performance characteristics with the thickness of the Ta<sub>2</sub>O<sub>5</sub> layer. Parameter values for a thickness of 0 nm correspond to that of the reference solar cell.

## EXPERIMENTAL DETAILS

For solar cell fabrication, 2  $\mu$ m thick undoped InP epitaxial films were grown using metal organic chemical vapor deposition (MOCVD) on p-doped (Zn: 3-5e18 /cm<sup>3</sup>) InP single side polished wafers. The ohmic back contacts to the InP wafers were made by DC sputtering of 20/100 nm Zn/Au films followed by annealing in H<sub>2</sub>+N<sub>2</sub> (5% H<sub>2</sub>) gas at 400 °C for 40 mins. Before depositing the back contact film, the native oxide layer on InP wafer was removed by dipping it in diluted HCl (6 to 7%) for one minute. A Ta<sub>2</sub>O<sub>5</sub> layer was then deposited on the front side of the wafer using an atomic layer deposition (ALD) system. Tantalum ethoxide maintained at 195 °C and H<sub>2</sub>O at 25 °C were used as tantalum and oxygen precursors, respectively, while the temperature of the deposition chamber was maintained at 225 °C. Ellipsometry (JA Woollam M-2000D) was used to calibrate the thickness of the Ta<sub>2</sub>O<sub>5</sub> films. In the next step, indium tin oxide (ITO) was deposited at room temperature using RF magnetron sputtering. The thickness of the ITO was adjusted so that the total thickness of the Ta<sub>2</sub>O<sub>5</sub> and ITO was maintained at a constant value of 70 nm to minimize reflections from the solar cell surface in the visible region of the solar spectrum. Front contacts were fabricated using photolithography followed by a metal lift-off process on a 200 nm e-beam evaporated silver

(Ag) layer. This process created a Ag grid on top of the ITO with a fringe width of 11  $\mu\text{m}$  and a spacing of 490  $\mu\text{m}$ . The area of the solar cell including the outer edge bus bar of the Ag grid was 1 cm  $\times$  1 cm. A schematic of the processing steps involved in the solar cell fabrication is shown in supporting information (Figure s1). A reference solar cell without the Ta<sub>2</sub>O<sub>5</sub> layer was also fabricated following the above processing steps.

A Perkin Elmer Lambda 1050 UV/Vis/NIR spectrophotometer was used for reflectance and transmission measurements of the solar cells. The photovoltaic performance of the solar cells was investigated under simulated one sun illumination using a Newport solar simulator equipped with an AM1.5G filter. The solar simulator power was calibrated against a commercial solar cell using their J-V measurements. A QE measurement system from Protoflex Corporation (QE-1400-03) was employed to study the quantum efficiency of the solar cells.

Transmission electron microscopy (TEM) was carried out using a JEOL 2100F instrument operated at 200 keV for structural characterization and energy dispersive X-ray spectroscopy (EDS) analysis of the Ta<sub>2</sub>O<sub>5</sub> layer used in the solar cells. A focused ion beam (FEI Helios 600 NanoLab) was used for the preparation of the cross sectional TEM lamella of the solar cell by using a Ga beam and an *in situ* lift-out process. Prior to the sample preparation, a layer of Pt was deposited on top of the solar cell using a FEI Helios 600 NanoLab ion beam deposition system to avoid any damage to the device layers from Ga ion milling.

A Thermo ESCALAB250Xi X-ray photoelectron spectrometer (XPS) with a monochromatic Al K-alpha X-ray source was employed for stoichiometric analysis and measurements of the valence band spectra of Ta<sub>2</sub>O<sub>5</sub> and InP. This equipment was operated in ultraviolet photoelectron spectroscopy (UPS) mode, using Helium I (21.2 eV) as the UV source, to measure the work function of Ta<sub>2</sub>O<sub>5</sub> and InP.

Power dependent photoluminescence and time-resolved photoluminescence (TRPL) measurements of InP and InP-Ta<sub>2</sub>O<sub>5</sub> samples were carried out at room temperature using a 522 nm wavelength pulsed laser excitation, which was generated by a BBO crystal through frequency doubling of an Yb:YAG laser. The excitation pulse had a duration of 300 fs and a repetition rate of 20.8 MHz. The laser beam was focused on the sample through a 100x (NA 0.75) microscope objective lens and the emitted light from the sample was also collected by the same lens. For lifetime measurements, the collected light from the objective lens was transferred to a single photon avalanche diode, which was connected to a PicoHarp 300 time-correlated single photon counting (TCSPC) system.

## CONCLUSIONS

View Article Online  
DOI: 10.1039/C8NR09932D

In summary, our work establishes stoichiometric Ta<sub>2</sub>O<sub>5</sub> as a promising carrier-selective (electron-transparent, hole-blocking) layer for InP heterojunction solar cells. We calculated the conduction band offset and valence band offset at the InP-Ta<sub>2</sub>O<sub>5</sub> interface to be 0.12 and 2.67 eV respectively using XPS and UPS measurements. The favourable band offsets enable efficient separation of photo-generated electrons and holes into the Ta<sub>2</sub>O<sub>5</sub> and InP layers respectively at the InP-Ta<sub>2</sub>O<sub>5</sub> interface. Using an ALD-deposited ultra-thin Ta<sub>2</sub>O<sub>5</sub> layer, we demonstrated an efficiency of 19.1% in a planar InP solar cell with the highest ever reported open circuit voltage, V<sub>oc</sub>, of 822 mV for an InP heterojunction solar cell with carrier-selective contacts. This work paves way for the development of novel solar cell architectures using Ta<sub>2</sub>O<sub>5</sub> electron-selective contacts that have the potential to achieve very high efficiencies. The ultrathin Ta<sub>2</sub>O<sub>5</sub> films may also attract attention in photoelectrochemical applications and interfacial engineering.

## ACKNOWLEDGEMENTS

We acknowledge the Australian Research Council (ARC) for financial support. Access to the epitaxy and device fabrication facilities is made possible through the Australian National Fabrication Facility (ANFF), ACT node.

## REFERENCES

1. Miles, R. W.; Zoppi, G.; Forbes, I., Inorganic photovoltaic cells. *Materials Today* **2007**, *10* (11), 20-27.
2. Green, M. A.; Hishikawa, Y.; Dunlop, E. D.; Levi, D. H.; Hohl-Ebinger, J.; Ho-Baillie, A. W. Y., Solar cell efficiency tables (version 52). *Progress in Photovoltaics: Research and Applications* **2018**, *26* (7), 427-436.
3. Kayes, B. M.; Nie, H.; Twist, R.; Spruytte, S. G.; Reinhardt, F.; Kizilyalli, I. C.; Higashi, G. S. In *27.6% Conversion efficiency, a new record for single-junction solar cells under 1 sun illumination*, 2011 37th IEEE Photovoltaic Specialists Conference, 19-24 June 2011; 2011; pp 000004-000008.
4. Green, M. A.; Emery, K.; Hishikawa, Y.; Warta, W.; Dunlop, E. D., Solar cell efficiency tables (version 48). *Progress in Photovoltaics: Research and Applications* **2016**, *24* (7), 905-913.
5. Keavney, C. J.; Haven, V. E.; Vernon, S. M. In *Emitter structures in MOCVD InP solar cells*, IEEE Conference on Photovoltaic Specialists, 21-25 May 1990; 1990; pp 141-144 vol.1.
6. Hettick, M.; Zheng, M.; Lin, Y.; Sutter-Fella, C. M.; Ager, J. W.; Javey, A., Nonepitaxial Thin-Film InP for Scalable and Efficient Photocathodes. *The Journal of Physical Chemistry Letters* **2015**, *6* (12), 2177-2182.

7. Eyderman, S.; John, S., Light-trapping and recycling for extraordinary power conversion in ultra-thin gallium-arsenide solar cells. *Scientific reports* **2016**, *6*, 28303. View Article Online  
DOI: 10.1039/C6NR09932D
8. Schermer, J. J.; Mulder, P.; Bauhuis, G. J.; Larsen, P. K.; Oomen, G.; Bongers, E., Thin-film GaAs epitaxial lift-off solar cells for space applications. *Progress in Photovoltaics: Research and Applications* **2005**, *13* (7), 587-596.
9. Bauhuis, G. J.; Mulder, P.; Haverkamp, E. J.; Schermer, J. J.; Bongers, E.; Oomen, G.; Köstler, W.; Strobl, G., Wafer reuse for repeated growth of III–V solar cells. *Progress in Photovoltaics: Research and Applications* **2010**, *18* (3), 155-159.
10. Yin, X.; Battaglia, C.; Lin, Y.; Chen, K.; Hettick, M.; Zheng, M.; Chen, C.-Y.; Kiriya, D.; Javey, A., 19.2% Efficient InP Heterojunction Solar Cell with Electron-Selective TiO<sub>2</sub> Contact. *ACS Photonics* **2014**, *1* (12), 1245-1250.
11. Saito, S.; Hashimoto, Y.; Ito, K. In *Efficient ZnO/CdS/InP heterojunction solar cell*, Proceedings of 1994 IEEE 1st World Conference on Photovoltaic Energy Conversion - WCPEC (A Joint Conference of PVSC, PVSEC and PSEC), 5-9 Dec 1994; 1994; pp 1867-1870 vol.2.
12. Shockley, W.; Queisser, H. J., Detailed Balance Limit of Efficiency of p-n Junction Solar Cells. *Journal of Applied Physics* **1961**, *32* (3), 510-519.
13. Peter Würfel, U. W., *Physics of Solar Cells: From Basic Principles to Advanced Concepts*. Wiley-VCH Weinheim, Germany, 2016; p 256.
14. Richter, A.; Glunz, S. W.; Werner, F.; Schmidt, J.; Cuevas, A., Improved quantitative description of Auger recombination in crystalline silicon. *Physical Review B* **2012**, *86* (16), 165202.
15. Min, B.; Wagner, H.; Dastgheib-Shirazi, A.; Kimmerle, A.; Kurz, H.; Altermatt, P. P., Heavily doped Si:P emitters of crystalline Si solar cells: recombination due to phosphorus precipitation. *physica status solidi (RRL) – Rapid Research Letters* **2014**, *8* (8), 680-684.
16. Schmidt, J.; Cuevas, A., Electronic properties of light-induced recombination centers in boron-doped Czochralski silicon. *Journal of Applied Physics* **1999**, *86* (6), 3175-3180.
17. King, R. R.; Sinton, R. A.; Swanson, R. M., Studies of diffused phosphorus emitters: saturation current, surface recombination velocity, and quantum efficiency. *IEEE Transactions on Electron Devices* **1990**, *37* (2), 365-371.
18. Yan, D.; Cuevas, A., Empirical determination of the energy band gap narrowing in p+ silicon heavily doped with boron. *Journal of Applied Physics* **2014**, *116* (19), 194505.
19. Taguchi, M.; Yano, A.; Tohoda, S.; Matsuyama, K.; Nakamura, Y.; Nishiwaki, T.; Fujita, K.; Maruyama, E., 24.7% Record Efficiency HIT Solar Cell on Thin Silicon Wafer. *IEEE Journal of Photovoltaics* **2014**, *4* (1), 96-99.
20. Deligiannis, D.; Marioleas, V.; Vasudevan, R.; Visser, C. C. G.; Swaaij, R. A. C. M. M. v.; Zeman, M., Understanding the thickness-dependent effective lifetime of crystalline silicon passivated with a thin layer of intrinsic hydrogenated amorphous silicon using a nanometer-accurate wet-etching method. *Journal of Applied Physics* **2016**, *119* (23), 235307.
21. Brendel, R.; Peibst, R., Contact Selectivity and Efficiency in Crystalline Silicon Photovoltaics. *IEEE Journal of Photovoltaics* **2016**, *6* (6), 1413-1420.
22. Battaglia, C.; Nicolás, S. M. d.; Wolf, S. D.; Yin, X.; Zheng, M.; Ballif, C.; Javey, A., Silicon heterojunction solar cell with passivated hole selective MoO<sub>x</sub> contact. *Applied Physics Letters* **2014**, *104* (11), 113902.

23. Battaglia, C.; Yin, X.; Zheng, M.; Sharp, I. D.; Chen, T.; McDonnell, S.; Azcatl, A.; Carraro, C.; Ma, B.; Maboudian, R.; Wallace, R. M.; Javey, A., Hole Selective MoOx Contact for Silicon Solar Cells. *Nano Letters* **2014**, *14* (2), 967-971. View Article Online  
DOI: 10.1039/C4NR09932D
24. Bullock, J.; Hettick, M.; Geissbühler, J.; Ong, A. J.; Allen, T.; Sutter-Fella, Carolin M.; Chen, T.; Ota, H.; Schaler, E. W.; De Wolf, S.; Ballif, C.; Cuevas, A.; Javey, A., Efficient silicon solar cells with dopant-free asymmetric heterocontacts. *Nature Energy* **2016**, *1*, 15031.
25. Bullock, J.; Wan, Y.; Xu, Z.; Essig, S.; Hettick, M.; Wang, H.; Ji, W.; Boccard, M.; Cuevas, A.; Ballif, C.; Javey, A., Stable Dopant-Free Asymmetric Heterocontact Silicon Solar Cells with Efficiencies above 20%. *ACS Energy Letters* **2018**, *3* (3), 508-513.
26. Geissbühler, J.; Werner, J.; Nicolas, S. M. d.; Barraud, L.; Hessler-Wyser, A.; Despeisse, M.; Nicolay, S.; Tomasi, A.; Niesen, B.; Wolf, S. D.; Ballif, C., 22.5% efficient silicon heterojunction solar cell with molybdenum oxide hole collector. *Applied Physics Letters* **2015**, *107* (8), 081601.
27. Lin, W.; Wu, W.; Liu, Z.; Qiu, K.; Cai, L.; Yao, Z.; Ai, B.; Liang, Z.; Shen, H., Chromium Trioxide Hole-Selective Heterocontacts for Silicon Solar Cells. *ACS Applied Materials & Interfaces* **2018**, *10* (16), 13645-13651.
28. Oener, S. Z.; Cavalli, A.; Sun, H.; Haverkort, J. E. M.; Bakkers, E. P. A. M.; Garnett, E. C., Charge carrier-selective contacts for nanowire solar cells. *Nature Communications* **2018**, *9* (1), 3248.
29. Wan, Y.; Bullock, J.; Hettick, M.; Xu, Z.; Samundsett, C.; Yan, D.; Peng, J.; Ye, J.; Javey, A.; Cuevas, A., Temperature and Humidity Stable Alkali/Alkaline-Earth Metal Carbonates as Electron Heterocontacts for Silicon Photovoltaics. *Advanced Energy Materials* **2018**, *8* (22), 1800743.
30. Wan, Y.; Samundsett, C.; Bullock, J.; Allen, T.; Hettick, M.; Yan, D.; Zheng, P.; Zhang, X.; Cui, J.; McKeon, J.; Javey, A.; Cuevas, A., Magnesium Fluoride Electron-Selective Contacts for Crystalline Silicon Solar Cells. *ACS Applied Materials & Interfaces* **2016**, *8* (23), 14671-14677.
31. Wan, Y.; Samundsett, C.; Bullock, J.; Hettick, M.; Allen, T.; Yan, D.; Peng, J.; Wu, Y.; Cui, J.; Javey, A.; Cuevas, A., Conductive and Stable Magnesium Oxide Electron-Selective Contacts for Efficient Silicon Solar Cells. *Advanced Energy Materials* **2017**, *7* (5), 1601863.
32. Yang, X.; Aydin, E.; Xu, H.; Kang, J.; Hedhili, M.; Liu, W.; Wan, Y.; Peng, J.; Samundsett, C.; Cuevas, A.; Wolf, S., Tantalum Nitride Electron-Selective Contact for Crystalline Silicon Solar Cells. *Advanced Energy Materials* **2018**, *8* (20), 1800608.
33. Wan, Y.; Karuturi, S. K.; Samundsett, C.; Bullock, J.; Hettick, M.; Yan, D.; Peng, J.; Narangari, P. R.; Mokkaapati, S.; Tan, H. H.; Jagadish, C.; Javey, A.; Cuevas, A., Tantalum Oxide Electron-Selective Heterocontacts for Silicon Photovoltaics and Photoelectrochemical Water Reduction. *ACS Energy Letters* **2018**, *3* (1), 125-131.
34. Battaglia, C.; de Nicolás, S. M.; De Wolf, S.; Yin, X.; Zheng, M.; Ballif, C.; Javey, A., Silicon heterojunction solar cell with passivated hole selective MoOx contact. *Applied Physics Letters* **2014**, *104* (11), 113902.
35. Islam, R.; Saraswat, K. C. In *Metal/insulator/semiconductor carrier selective contacts for photovoltaic cells*, 2014 IEEE 40th Photovoltaic Specialist Conference (PVSC), 8-13 June 2014; 2014; pp 0285-0289.

36. Bullock, J.; Cuevas, A.; Allen, T.; Battaglia, C., Molybdenum oxide MoO<sub>x</sub>: A versatile hole contact for silicon solar cells. *Applied Physics Letters* **2014**, *105* (23), 232109. View Article Online  
DOI: 10.1039/C3NR09932D
37. Bivour, M.; Temmler, J.; Steinkemper, H.; Hermle, M., Molybdenum and tungsten oxide: High work function wide band gap contact materials for hole selective contacts of silicon solar cells. *Solar Energy Materials and Solar Cells* **2015**, *142*, 34-41.
38. Wang, F.; Zhao, S.; Liu, B.; Li, Y.; Ren, Q.; Du, R.; Wang, N.; Wei, C.; Chen, X.; Wang, G.; Yan, B.; Zhao, Y.; Zhang, X., Silicon solar cells with bifacial metal oxides carrier selective layers. *Nano Energy* **2017**, *39*, 437-443.
39. Tong, J.; Wan, Y.; Cui, J.; Lim, S.; Song, N.; Lennon, A., *Solution-processed Molybdenum Oxide for Hole-selective Contacts on Crystalline Silicon Solar Cells*. 2017; Vol. 423.
40. Avasthi, S.; McClain, W. E.; Man, G.; Kahn, A.; Schwartz, J.; Sturm, J. C., Hole-blocking titanium-oxide/silicon heterojunction and its application to photovoltaics. *Applied Physics Letters* **2013**, *102* (20), 203901.
41. Novkovski, N.; Atanassova, E., Origin of the stress-induced leakage currents in Al-Ta<sub>2</sub>O<sub>5</sub>/SiO<sub>2</sub>-Si structures. *Applied Physics Letters* **2005**, *86* (15), 152104.
42. Joshi, P. C.; Cole, M. W., Influence of postdeposition annealing on the enhanced structural and electrical properties of amorphous and crystalline Ta<sub>2</sub>O<sub>5</sub> thin films for dynamic random access memory applications. *Journal of Applied Physics* **1999**, *86* (2), 871-880.
43. Chu, K.; Cho, B.-O.; Chang, J. P.; Steigerwald, M. L.; Fleming, R. M.; Opila, R. L.; Lang, D. V.; Dover, R. B. V.; Jones, C. D. W., Material and Electrical Characterization of Carbon-Doped Ta<sub>2</sub>O<sub>5</sub> Films for Embedded DRAM Applications. *MRS Proceedings* **2011**, 672.
44. Chun, W.-J.; Ishikawa, A.; Fujisawa, H.; Takata, T.; Kondo, J. N.; Hara, M.; Kawai, M.; Matsumoto, Y.; Domen, K., Conduction and Valence Band Positions of Ta<sub>2</sub>O<sub>5</sub>, TaON, and Ta<sub>3</sub>N<sub>5</sub> by UPS and Electrochemical Methods. *The Journal of Physical Chemistry B* **2003**, *107* (8), 1798-1803.
45. Nashed, R.; Hassan, W. M. I.; Ismail, Y.; Allam, N. K., Unravelling the interplay of crystal structure and electronic band structure of tantalum oxide (Ta<sub>2</sub>O<sub>5</sub>). *Physical Chemistry Chemical Physics* **2013**, *15* (5), 1352-1357.
46. Shvets, V. A.; Aliev, V. S.; Gritsenko, D. V.; Shaimeev, S. S.; Fedosenko, E. V.; Rykhliński, S. V.; Atuchin, V. V.; Gritsenko, V. A.; Tapilin, V. M.; Wong, H., Electronic structure and charge transport properties of amorphous Ta<sub>2</sub>O<sub>5</sub> films. *Journal of Non-Crystalline Solids* **2008**, *354* (26), 3025-3033.
47. Wan, Y.; Krishna Karuturi, S.; Samundsett, C.; Bullock, J.; Hettick, M.; Yan, D.; Peng, J.; Narangari, P. R.; Mokkapati, S.; Hoe Tan, H.; Jagadish, C.; Javey, A.; Cuevas, A., *Tantalum Oxide Electron-selective Heterocontacts for Silicon Photovoltaics and Photoelectrochemical Water Reduction*. 2017.
48. Kerrec, O.; Devilliers, D.; Groult, H.; Marcus, P., Study of dry and electrogenerated Ta<sub>2</sub>O<sub>5</sub> and Ta/Ta<sub>2</sub>O<sub>5</sub>/Pt structures by XPS. *Materials Science and Engineering: B* **1998**, *55* (1), 134-142.
49. Atanassova, E.; Dimitrova, T.; Koprinarova, J., AES and XPS study of thin RF-sputtered Ta<sub>2</sub>O<sub>5</sub> layers. *Applied Surface Science* **1995**, *84* (2), 193-202.

50. Spassov, E. A. D., X-ray photoelectron spectroscopy of thermal thin Ta<sub>2</sub>O<sub>5</sub> films on Si. *Applied Surface Science* **1998**, *135*. View Article Online  
DOI: 10.1039/C8NR09932D
51. Wagner, S.; Shay, J. L.; Bachmann, K. J.; Buehler, E., p-InP/n-CdS solar cells and photovoltaic detectors. *Applied Physics Letters* **1975**, *26* (5), 229-230.